EDGE ARTICLE

A hydrazone-based covalent organic framework for photocatalytic hydrogen production†

Linus Stegbauer,[abc] Katharina Schwinghammer[abc] and Bettina V. Lotsch*[abc]

Covalent organic frameworks (COFs) have recently emerged as a new generation of porous polymers combining molecular functionality with the robustness and structural definition of crystalline solids. Drawing on the recent development of tailor-made semiconducting COFs, we report here on a new COF capable of visible-light driven hydrogen generation in the presence of Pt as a proton reduction catalyst (PRC). The COF is based on hydrazone-linked functionalized triazine and phenyl building blocks and adopts a layered structure with a honeycomb-type lattice featuring mesopores of 3.8 nm and the highest surface area among all hydrazone-based COFs reported to date. When illuminated with visible light, the Pt-doped COF continuously produces hydrogen from water without signs of degradation. With their precise molecular organization and modular structure combined with high porosity, photoactive COFs represent well-defined model systems to study and adjust the molecular entities central to the photocatalytic process.

Introduction

The last decade has seen a continuous rise in activity revolving around the development of potent photocatalytic systems which are capable of transforming solar energy into chemical fuels.[1] Whilst most photocatalysts are based on inorganic semiconductors,[2] there are a few examples of materials composed solely of light elements.[3] These systems, prominently represented by carbon nitride polymers, are moderately active in hydrogen generation from water,[4] however their performance can be significantly enhanced by morphology tuning and structural modifications, including doping.[5,6] The major downside of these polymers, however, is their lack of crystallinity and generally low surface areas, which are inherently hard to control. In addition, carbon nitrides are invariably composed of heptazine or triazine units, thus offering only limited chemical variety and they are not very susceptible to systematic post-modification. A closely related class of organic polymers, dubbed covalent organic frameworks (COFs), is apt to overcome these inherent weaknesses of carbon nitrides by combining

chemical versatility and modularity with potentially high crystallinity and porosity.[7–11] Recently, unique 2D COFs with interesting optoelectronic properties have emerged, representing ideal scaffolds for exciton separation and charge percolation within self-sorted, nanoscale phase-separated architectures. Whereas most COFs rely on the formation of water-labile boronate ester linkages,[12] a few other examples based on imine[13–17] and hydrazone[18] linkages have been synthesized recently. For example, the imine-based COF-LZU1 in combination with Pd has been used as catalyst in Suzuki couplings.[19] Surprisingly, after the pioneering work by Yaghi, hydrazone formation has not been used again for the synthesis of COFs, although hydrazones are typically much less prone to hydrolysis than imines.[20] This chemoselective type of bond formation between a substituted acyl hydrazine and an aldehyde is highlighted by its use in labeling modified proteins[21] and for drug delivery purposes.[22]

Although big strides towards photoactive COFs with light-harvesting and charge separation capabilities have already been made,[15,23–27] COFs have not yet been explored as photosensitizers in photocatalytic systems for the production of solar fuels. A first indication of the underlying potential of COFs as a photoactive material was the light-induced activation of oxygen by a squaraine-based COF reported recently by Jiang and co-workers.[13]

Herein, we report the first COF which is active in visible light induced hydrogen evolution in the presence of Pt as the proton reduction catalyst (PRC). Our hydrazone-based COF (TFPT–COF) is constructed from 1,3,5-tris-(4-formyl-phenyl)triazine (TFPT) and 2,5-diethoxy-terephthalohydrazide (DETH) building blocks (Fig. 1), featuring mesopores of 3.8 nm in diameter and

aMax Planck Institute for Solid State Research, Heisenbergstr. 1, 70569 Stuttgart, Germany. E-mail: b.lotsch@fkf.mpg.de

bDepartment of Chemistry, University of Munich (LMU), Butenandtstr. 5-13, 81377 München, Germany

cNanosystems Initiative Munich (NIM) & Center for Nanoscience, Schellingstr. 4, 80799 München, Germany
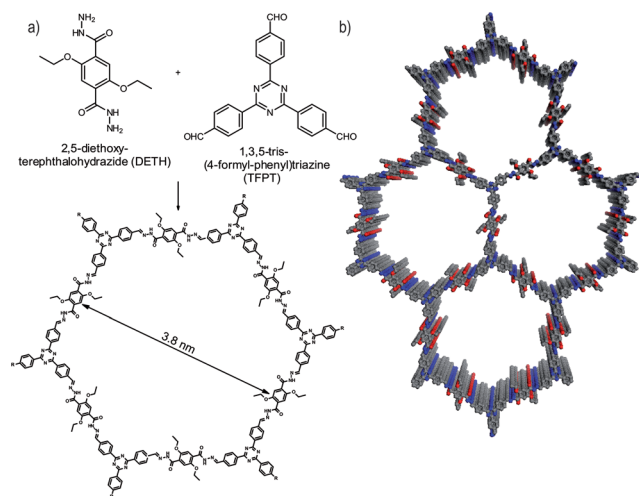
Fig. 1 Acetic acid catalysed hydrazone formation furnishes a mesoporous 2D network with a honeycomb-type in plane structure. (a) Scheme showing the condensation of the two monomers to form the TFPT–COF. (b) TFPT–COF with a cofacial orientation of the aromatic building blocks, constituting a close-to eclipsed primitive hexagonal lattice (grey: carbon, blue: nitrogen, red: oxygen).

the highest surface area among all hydrazone-based COFs reported so far.

Results and discussion

TFPT–COF: Synthesis and characterization

Triazine-based molecules offer high electron mobilities, electron withdrawing character[28] and are hence widely used in synthetic chemistry[29] and optoelectronics.[28] TFPT has a much smaller dihedral angle between the phenyl and triazine unit (~7.7°) compared to its benzene centered analogue (38.3°) (Fig. S1, ESI†).[30] As a consequence, the use of TFPT should facilitate the formation of a planar COF with an extended π-system compared to the monomers and enhanced crystallinity. Indeed, the TFPT–COF turns out to be crystalline and at the same time stable in methanol and other solvents (Fig. S15, ESI†).

TFPT–COF was synthesized by the acetic acid catalysed reversible condensation of the building blocks in dioxane–mesitylene (1 : 2 v/v) at 120 °C in a sealed pressure vial under an argon atmosphere for 72 hours. The product was obtained as a fluffy pale-yellow nanocrystalline solid. To remove any starting material or solvent contained in the pores, TFPT–COF was centrifuged, washed with DMF and THF, soaked in DCM for 3 hours, and subsequently heated to 120 °C under a high dynamic vacuum for 12 h (10^{-7} mbar).

It is worth mentioning that TFPT–COF could also be synthesized by *in situ* deprotection and subsequent condensation in a one-pot procedure (see Scheme S6, ESI†). Using this reaction scheme, the acetal protected TFPT is deprotected by treatment with a catalytic amount of camphorsulfonic acid in the solvent mixture. The COF formation is then started by adding the corresponding catalytic amount of sodium acetate to

the reaction mixture. After 72 h, we obtained a material chemically and structurally identical to TFPT–COF (Fig. S2, ESI†). This protocol opens the door to a new variety of acetal-protected building blocks and at the same time enhances the solubility of otherwise insoluble building blocks due to the aliphatic protection group.

ATR-IR data of TFTP-COF show stretching modes in the range 1670–1660 cm^{-1} and 1201–1210 cm^{-1}, which are characteristic of C≡N moieties. The lack of the aldehyde Fermi double resonance at 2824 and 2721 cm^{-1}, as well as the aldehyde carbonyl stretching vibration at 1700 cm^{-1} of the TFPT monomer clearly suggests the absence of any starting material. Furthermore, the triazine moiety is still present in the TFTP-COF as ascertained by the triazine semicircle stretch vibration at 806 cm^{-1} (Fig. S3†).

^{1}H solid-state NMR MAS spectroscopy shows the presence of the ethoxy group through signals at 1.39 ppm (CH_3–CH_2–O) and 3.29 ppm (CH_3–CH_2–O) (Fig. 2e). The aromatic region is represented by a broadened signal at 6.5 ppm. Furthermore, the ^{13}C CP-MAS spectrum clearly supports the formation of a hydrazone bond corresponding to the signal at 148.9 ppm, and confirms the presence of the triazine ring (167.9 ppm) (Fig. 2d). All other signals were also unambiguously assigned to the corresponding carbon atoms (Fig. 2c).[18]

Powder X-ray diffraction (PXRD) measurements confirm the formation of a crystalline framework with metrics being consistent with the structure model shown in Fig. 1. Comparison of the experimental data with the simulation[31] reveal a hexagonal structure with *P6/m* symmetry and an eclipsed AA layer stacking, which is in line with most COF structures reported to date (Fig. 2a).[7–11] Nevertheless, we assume that slight offsets with respect to the ideal cofacial layer stacking have to be
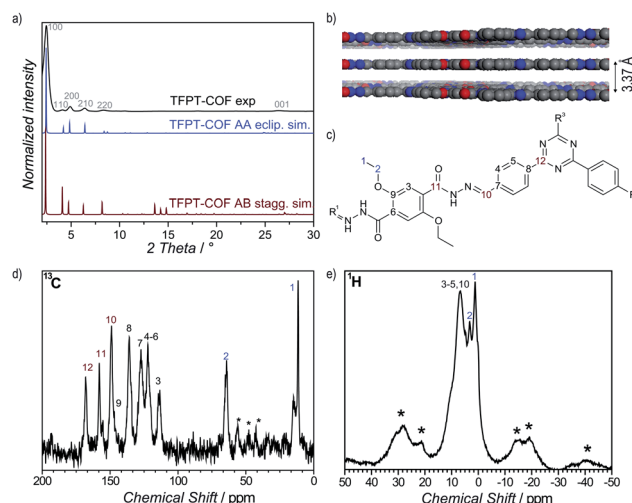

Fig. 2 Characterization of the TFPT–COF by PXRD and MAS solid-state NMR spectroscopy. (a) and (b) PXRD suggests a (close to) eclipsed layer stacking as confirmed by Pawley refinement of the AA-stacked structure model. (c) Assignment of ^{13}C and ^{1}H NMR data. (d) ^{13}C CP-MAS NMR spectrum, asterisks mark spinning side bands. (e) ^{1}H MAS NMR spectrum with a group of signals centered between 1 and 8 ppm; asterisks mark spinning side bands.

taken into account as recently delineated by Heine,[32] Dichtel and co-workers.[33] Subtle layer offsets which are not resolvable by XRD result in the minimization of repulsive electrostatic forces between the layers with respect to the energetically less favorable, fully eclipsed structures. Nevertheless, whether the same situation also holds true for hydrazone COFs has yet to be demonstrated.

Pawley refinement (including peak broadening) of the experimental powder pattern gave lattice parameters of $a = b = 41.90$ Å (Fig. 2a and S5, ESI†). The theoretical powder pattern of the related staggered conformation derived from the *gra* net with $P6_3/m$ symmetry does not reproduce the observed intensity distribution and was therefore discarded (Fig. 2a and S8, ESI†). The 001 diffraction peak at $2\theta = 26.6$ corresponds to an interlayer distance of 3.37 Å (Fig. 2b), suggesting a typical van der Waals contact between the aromatic layers. Interestingly, the presence of the ethoxy groups protruding into the pores does not notably increase the interlayer distance, thus indicating a predominantly coplanar arrangement with the plane of the honeycomb lattice.

According to the above theoretical studies and other predictions for the stacking of triazines by Gamez *et al.*,[34] we have also simulated a parallel displaced structure (displacement vector 1.4 Å) with an AA′A-type stacking sequence (Fig. S9 and S10, ESI†). As expected, the simulated PXRD is very similar to both the experimental PXRD as well as the PXRD calculated for the perfectly eclipsed structure (Fig. S11, ESI†).

Argon sorption measurements at 87 K clearly show the formation of mesopores as indicated by a typical type IV adsorption isotherm (Fig. 3a). The Brunauer–Emmett–Teller (BET) surface area was calculated to be 1603 m² g⁻¹ (total pore volume is 1.03 cm³ g⁻¹, Fig. S12, ESI†), which is the highest measured surface area among all hydrazone COFs reported to date.[13–18,35] Comparing these values with those of COF-43, derived from a benzene-centered trigonal building block with the same pore size,[18] the surface area has more than doubled, probably as a consequence of the smaller dihedral angle of the triazine-centered TFPT and the resulting more favorable stacking interactions, or due to the more complete activation of the material. The pore size distribution (PSD) was evaluated with non-local density functional theory (NLDFT). The experimental

PSD exhibits a maximum at 3.8 nm, thereby verifying the theoretical pore diameter of 3.8 nm (Fig. S13, ESI†) which is the same pore size found by Yaghi and co-workers for their benzene-centered COF.[18] Transmission electron microscopy images confirm the data derived from PXRD and sorption measurements. The hexagonal pore arrangement with pore distances of ≈3.4 nm is clearly visible, as well as the layered nanomorphology (Fig. 3b).

The diffuse reflectance UV/Vis spectrum of the yellow powder exhibits an absorption edge around 400 nm (the spike at 380 nm is due to a change of the light source), with the absorption tail extending well beyond 600 nm (Fig. 4a). We estimate an optical band gap of roughly 2.8 eV from the absorption edge, based on the Kubelka–Munk function (Fig. S14, ESI†). The TFPT–COF shows a pronounced red-shift of the absorption edge by 33 nm in comparison with the individual building blocks. A similar broadened and red-shifted absorption of the COF with respect to the monomers has been found by Jiang and co-workers for several COF systems.[13,23–27] In principle, the observed HOMO–LUMO gap of the TFPT–COF is large enough to enable water splitting through band gap excitation and at the same time small enough to harvest a significant portion of the visible light spectrum.

To investigate this possibility, we studied the light-induced hydrogen evolution mediated by Pt-modified TFPT–COF in the presence of a sacrificial electron donor as the photocatalytic system under visible light irradiation. While TFPT–COF primarily acts as a photosensitizer for exciton generation, Pt functions as PRC. We previously demonstrated that the

Fig. 4 Optical properties of the TFPT–COF and photocatalytic hydrogen evolution. (a) UV/Vis diffuse reflectance spectra of TFPT–COF (black) and its monomers (blue and red). (b) Time course of hydrogen evolution from an aqueous sodium ascorbate solution by the Pt-modified TFPT–COF under visible light irradiation ($\lambda > 420$ nm). The inset shows the hydrogen evolution rate (19.7 μmol h⁻¹) from 10 vol% aqueous triethanolamine solution over 5 h (red). (c) Overlay of UV/Vis absorption of TFPT–COF and wavelength-specific hydrogen production of Pt-modified TFPT–COF in a 10 vol% aqueous triethanolamine solution using 40 nm FWHM band-pass filters. (d) TEM image of TFPT–COF/Pt after illumination for 84 h showing the formation of Pt nanoparticles (5 nm).
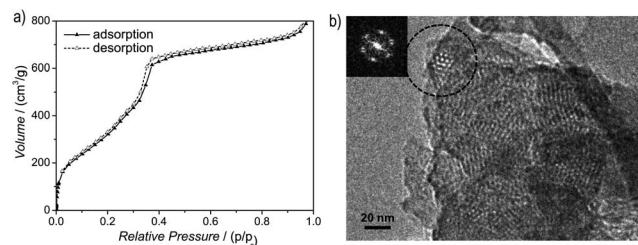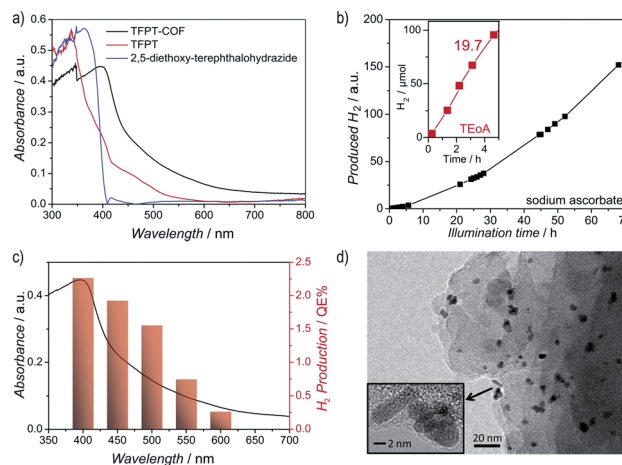

Fig. 3 Structural characterization of TFPT–COF by physisorption and TEM. (a) The argon-sorption isotherm shows the formation of mesopores, consistent with the predicted pore size based on the structure model. The reversible type IV isotherm (adsorption: black triangles, desorption: white triangles) gives a BET surface of 1603 m² g⁻¹. (b) TEM image showing the formation of hexagonal pores.
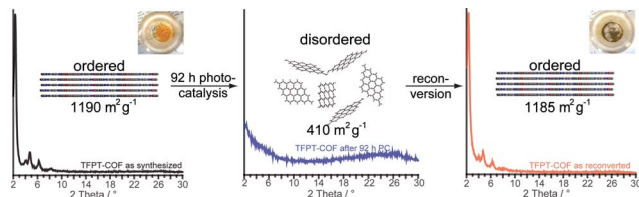
Fig. 5 Transformation of TFPT–COF during photocatalysis and subsequent recovery by reconversion (see ESI† for details). Inset photographs show colour change from yellow (TFPT–COF) to green (TFPT–COF/Pt).

Pt-modified triazine-based carbon nitride poly(triazine imide) (PTI) shows substantial photocatalytic activity, despite its amorphous character.[6] Therefore, the presence of triazine moieties in the TFPT–COF, along with a moderate band gap, renders this crystalline COF an excellent candidate to study hydrogen-evolution and possible structure–property relationships.

Photocatalytic hydrogen evolution

Hydrogen evolution was studied under standardized conditions and measured in the presence of the PRC Pt, using sodium ascorbate as sacrificial electron donor (see ESI† for details). In fact, TFPT–COF/Pt is a potent photocatalytic system, showing continuous and stable hydrogen production of 230 μmol h^{-1} g^{-1} (Fig. 4b and S22, ESI†). The total amount of hydrogen produced after 52 h (with sodium ascorbate) exceeds the total amount of hydrogen incorporated in the material (97.6 μmol), which adds evidence that hydrogen evolution is in fact catalytic and does not result from stoichiometric decomposition of the COF itself. Measurements in the dark (Fig. S22, ESI†) show no hydrogen evolution, confirming that the evolution of hydrogen is a photoinduced effect. The monomer TFPT alone does not show photocatalytic activity under these conditions either. The long-time stability was tested by catalyst cycling, *i.e.* centrifugation of the reaction mixture, washing of the precipitate and addition of fresh sodium ascorbate solution. Even after three cycles the hydrogen evolution does not decrease (Fig. S23, ESI†). Small fluctuations are due to small concentration differences of the COF/aqueous sodium ascorbate suspensions.

Using a 10 vol% aqueous triethanolamine (TEOA) solution as sacrificial donor, an even higher hydrogen evolution rate was detected, with the amount of hydrogen evolved in the first five hours being as high as 1970 μmol h^{-1} g^{-1}, corresponding to a quantum efficiency of 2.2%, while maximum QEs of up to 3.9% were obtained for individual batches (Fig. 4b). However, this high rate comes along with a quicker deactivation of the photocatalytic system. By reducing the amount of triethanolamine (1 vol%) and adjusting the suspension to pH = 7, stable hydrogen evolution for a longer time range (24 hours) was detected.

The observed high amount of hydrogen evolved under standard basic conditions (1970 μmol h^{-1} g^{-1}) suggests that TFPT–COF/Pt is superior to Pt-modified amorphous melon, g-C$_3$N$_4$ (which was synthesized according to Zhang *et al.*[5] at

600 °C) and crystalline poly(triazine imide) (720 μmol h^{-1} g^{-1}, 840 μmol h^{-1} g^{-1} and 864 μmol h^{-1} g^{-1}, respectively),[6] which were tested under similar conditions for three hours with TEOA as sacrificial donor. We also studied oxygen evolution to probe whether full water splitting is possible with the TFPT–COF. However, no O$_2$ could be detected under the conditions used (see ESI†).

Reconversion of TFPT–COF

After photocatalysis, the amorphous material was coated with dispersed Pt nanoparticles, formed *in situ* (Fig. 4d). The TEM images suggest that the material loses its long-range order during photocatalysis (Fig. 4d), which is supported by XRD measurements (Fig. 5 and S16, ESI†). This loss of long-range order has also been observed by Dichtel and co-workers and has been assigned to exfoliation of the COF in water.[20] To test this hypothesis, we carried out sorption measurements and PXRD after photocatalysis (95 h of irradiation in sodium ascorbate solution). TFPT–COF/Pt was filtered off as a greenish solid (Fig. 5, inset picture, see ESI† for more images). A DCM extract of the solid catalyst did not contain any molecular material, which suggests that the as-obtained powder did not decompose and no monomers were released. At the same time, however, crystallinity was lost (Fig. S16, ESI†) and the BET surface area was reduced to 410 m^2 g^{-1} (Fig. S18, ESI†). Nevertheless, we found that the amorphous product can easily be reconverted into the crystalline and porous TFPT–COF with a BET surface area of 1185 m^2 g^{-1} (Fig. 5 and ESI†) by subjecting it to the initial synthesis conditions. Further experiments revealed that the TFPT–COF loses its long-range order during sonication in water. Overall, this observation strengthens the hypothesis that the COF is exfoliated in water,[20] thereby losing its long-range order, while the connectivity and photoactivity is retained.

Conclusion

In conclusion, we have developed a new crystalline hydrazone-based TFPT–COF, which is the first COF to show photocatalytic hydrogen evolution under visible light irradiation in the presence of Pt as PRC. This framework is competitive with the best non-metal photocatalysts for hydrogen production and represents a lightweight, well-ordered model system, which in principle can be readily tuned – by replacement, expansion or chemical modification of its building blocks – to further study and optimize the underlying mechanism of hydrogen evolution mediated by the framework and to enhance its light harvesting capability. The triazine moieties in the TFPT–COF, which are likewise present in the recently developed triazine-based carbon nitride photocatalytic system PTI/Pt, may point to an active role of the triazine unit in the photocatalytic process.

The development of COFs as tunable scaffolds for photocatalytic hydrogen evolution enables a general bottom-up approach toward designing tailor-made photosensitizers and photocatalysts with tunable optical and electronic properties, a goal we are currently pursuing in our lab. We expect this new application of COFs in photocatalysis to open new avenues to

custom-made heterogeneous photocatalysts, and to direct and diversify the ongoing development of COFs for optoelectronic applications.

Acknowledgements

Notes and references

1 X. Chen, S. Shen, L. Guo and S. S. Mao, *Chem. Rev.*, 2010, **110**, 6503–6570.

2 H. Tong, S. Ouyang, Y. Bi, N. Umezawa, M. Oshikiri and J. Ye, *Adv. Mater.*, 2012, **24**, 229–251.

3 (*a*) S. Yanagida, A. Kabumoto, K. Mizumoto, C. Pac and K. Yoshino, *J. Chem. Soc., Chem. Commun.*, 1985, 474–475; (*b*) J. Liu, S. Wen, Y. Hou, F. Zuo, G. J. O. Beran and P. Feng, *Angew. Chem., Int. Ed.*, 2013, **52**, 3241–3245; (*c*) X. Wang, K. Maeda, A. Thomas, K. Takanabe, G. Xin, J. M. Carlsson, K. Domen and M. Antonietti, *Nat. Mater.*, 2009, **8**, 76–80.

4 K. Maeda, X. Wang, Y. Nishihara, D. Lu, M. Antonietti and K. Domen, *J. Phys. Chem. C*, 2009, **113**, 4940–4947.

5 J. Zhang, X. Chen, K. Takanabe, K. Maeda, K. Domen, J. D. Epping, X. Fu, M. Antonietti and X. Wang, *Angew. Chem., Int. Ed.*, 2010, **49**, 441–444.

6 K. Schwinghammer, B. Tuffy, M. B. Mesch, E. Wirnhier, C. Martineau, F. Taulelle, W. Schnick, J. Senker and B. V. Lotsch, *Angew. Chem., Int. Ed.*, 2013, **52**, 2435–2439.

7 A. P. Côté, A. I. Benin, N. W. Ockwig, M. O'Keeffe, A. J. Matzger and O. M. Yaghi, *Science*, 2005, **310**, 1166–1170.

8 H. M. El-Kaderi, J. R. Hunt, J. L. Mendoza-Cortes, A. P. Côté, R. E. Taylor, M. O'Keeffe and O. M. Yaghi, *Science*, 2007, **316**, 268–272.

9 A. P. Côté, H. M. El-Kaderi, H. Furukawa, J. R. Hunt and O. M. Yaghi, *J. Am. Chem. Soc.*, 2007, **129**, 12914–12915.

10 S.-Y. Ding and W. Wang, *Chem. Soc. Rev.*, 2013, **42**, 548–568.

11 X. Feng, X. Ding and D. Jiang, *Chem. Soc. Rev.*, 2012, **41**, 6010–6022.

12 Y. Du, K. Mao, P. Kamakoti, P. Ravikovitch, C. Paur, S. Cundy, Q. Li and D. Calabro, *Chem. Commun.*, 2012, **48**, 4606–4608.

13 A. Nagai, X. Chen, X. Feng, X. Ding, Z. Guo and D. Jiang, *Angew. Chem., Int. Ed.*, 2013, **52**, 3770–3774.

14 X. Chen, M. Addicoat, S. Irle, A. Nagai and D. Jiang, *J. Am. Chem. Soc.*, 2012, **135**, 546–549.

15 S. Wan, F. Gándara, A. Asano, H. Furukawa, A. Saeki, S. K. Dey, L. Liao, M. W. Ambrogio, Y. Y. Botros, X. Duan, S. Seki, J. F. Stoddart and O. M. Yaghi, *Chem. Mater.*, 2011, **23**, 4094–4097.

16 F. J. Uribe-Romo, J. R. Hunt, H. Furukawa, C. Klöck, M. O'Keeffe and O. M. Yaghi, *J. Am. Chem. Soc.*, 2009, **131**, 4570–4571.

17 M. G. Rabbani, A. K. Sekizkardes, Z. Kahveci, T. E. Reich, R. Ding and H. M. El-Kaderi, *Chem.–Eur. J.*, 2013, **19**, 3324–3328.

18 F. J. Uribe-Romo, C. J. Doonan, H. Furukawa, K. Oisaki and O. M. Yaghi, *J. Am. Chem. Soc.*, 2011, **133**, 11478–11481.

19 S.-Y. Ding, J. Gao, Q. Wang, Y. Zhang, W.-G. Song, C.-Y. Su and W. Wang, *J. Am. Chem. Soc.*, 2011, **133**, 19816–19822.

20 D. N. Bunck and W. R. Dichtel, *J. Am. Chem. Soc.*, 2013, **135**, 14952–14955.

21 T. P. King, S. W. Zhao and T. Lam, *Biochemistry*, 1986, **25**, 5774–5779.

22 C. C. Lee, E. R. Gillies, M. E. Fox, S. J. Guillaudeu, J. M. J. Fréchet, E. E. Dy and F. C. Szoka, *Proc. Natl. Acad. Sci. U. S. A.*, 2006, **103**, 16649–16654.

23 S. Jin, X. Ding, X. Feng, M. Supur, K. Furukawa, S. Takahashi, M. Addicoat, M. E. El-Khouly, T. Nakamura, S. Irle, S. Fukuzumi, A. Nagai and D. Jiang, *Angew. Chem., Int. Ed.*, 2013, **52**, 2017–2021.

24 E. L. Spitler and W. R. Dichtel, *Nat. Chem.*, 2010, **2**, 672–677.

25 X. Ding, X. Feng, A. Saeki, S. Seki, A. Nagai and D. Jiang, *Chem. Commun.*, 2012, **48**, 8952–8954.

26 X. Ding, J. Guo, X. Feng, Y. Honsho, J. Guo, S. Seki, P. Maitarad, A. Saeki, S. Nagase and D. Jiang, *Angew. Chem., Int. Ed.*, 2011, **50**, 1289–1293.

27 X. Ding, L. Chen, Y. Honsho, X. Feng, O. Saengsawang, J. Guo, A. Saeki, S. Seki, S. Irle, S. Nagase, V. Parasuk and D. Jiang, *J. Am. Chem. Soc.*, 2011, **133**, 14510–14513.

28 T. Ishi-i, K. Yaguma, T. Thiemann, M. Yashima, K. Ueno and S. Mataka, *Chem. Lett.*, 2004, **33**, 1244–1245.

29 D. Sun, S. Ma, Y. Ke, D. J. Collins and H.-C. Zhou, *J. Am. Chem. Soc.*, 2006, **128**, 3896–3897.

30 (*a*) Z.-S. Li, J.-X. Chen, Y.-B. Huang, G.-R. Chen and T.-Y. Lan, *Acta Crystallogr., Sect. E: Struct. Rep. Online*, 2006, **62**, 777–779; (*b*) V. Volkis, E. Nelkenbaum, A. Lisovskii, G. Hasson, R. Semiat, M. Kapon, M. Botoshansky, Y. Eishen and M. S. Eisen, *J. Am. Chem. Soc.*, 2003, **125**, 2179–2194.

31 *Material Studio v. 5.5.0.0*, Accelrys Software Inc., 2011.

32 B. Lukose, A. Kuc and T. Heine, *Chem.–Eur. J.*, 2011, **17**, 2388–2392.

33 B. T. Koo, W. R. Dichtel and P. Clancy, *J. Mater. Chem.*, 2012, **22**, 17460–17469.

34 (*a*) S. Grimme, *Angew. Chem., Int. Ed.*, 2008, **47**, 3430–3434; (*b*) J. Antony, B. Alameddine, T. A. Jenny and S. Grimme, *J. Phys. Chem. A*, 2012, **117**, 616–625; (*c*) T. J. Mooibroek and P. Gamez, *Inorg. Chim. Acta*, 2007, **360**, 381–404; (*d*) W. Pisula, H. Tsao, D. Dudenko, D. Cho, S. Puniredd, Y. Zhao, A. Mavrinskiy, J. Shu, M. Hansen, M. Baumgarten and K. Müllen, *Polymers*, 2013, **5**, 833–846.

35 (*a*) S. Chandra, S. Kandambeth, B. P. Biswal, B. Lukose, S. M. Kunjir, M. Chaudhary, R. Babarao, T. Heine and R. Banerjee, *J. Am. Chem. Soc.*, 2013, **135**, 17853–17861; (*b*) S. Kandambeth, D. B. Shinde, M. K. Panda, B. Lukose, T. Heine and R. Banerjee, *Angew. Chem., Int. Ed.*, 2013, **52**, 13052–13056; (*c*) S. Kandambeth, A. Mallick, B. Lukose, M. V. Mane, T. Heine and R. Banerjee, *J. Am. Chem. Soc.*, 2012, **134**, 19524–19527.